


Detachment between edge and skin states in a non-Hermitian latticeZhi-Xu Zhang,¹ Ji Cao,² Wen-Xue Cui², Yu Zhang,^{1,*} Shou Zhang,^{2,†} and Hong-Fu Wang^{2,‡}¹*School of Physics, Harbin Institute of Technology, Harbin, Heilongjiang 150001, China*²*Department of Physics, College of Science, Yanbian University, Yanji, Jilin 133002, China* (Received 22 June 2023; revised 27 September 2023; accepted 26 October 2023; published 9 November 2023)

The integration of nonreciprocal non-Hermiticity and topological lattice systems can induce the emergence of the non-Hermitian skin effect, enabling a clear distinction between the behaviors of bulk states in non-Hermitian systems and those in Hermitian systems. Specifically, we focus on examining the localized directions of eigenstates in an odd-sized Su-Schrieffer-Heeger-type lattice with intracell nonreciprocal hopping, and identify a notable phenomenon of detachment between the edge and bulk states, which stands in stark contrast to the behaviors observed in even-sized cases. The localized directions of the bulk and edge states are respectively subjected to the non-Hermitian skin effect and isolated site induced by the odd size of the lattice, resulting in the detachment between the edge and skin states. To provide a comprehensive understanding of the detachment phenomenon, we present analytical solutions that illustrate the localized directions of the edge and skin states whose results are in perfect agreement with the numerical findings. Furthermore, we demonstrate that a pair of eigenstates exhibiting opposite localized directions to the skin states can appear in a trimer non-Hermitian lattice, indicating the possibility of detachment between the edge and skin states in multimer non-Hermitian lattices as well.

DOI: [10.1103/PhysRevA.108.052210](https://doi.org/10.1103/PhysRevA.108.052210)**I. INTRODUCTION**

Since the discovery of topological insulators, there has been significant interest in studying topological phases [1–3]. Among these efforts, the Su-Schrieffer-Heeger (SSH) model holds a prominent position owing to its succinct band structure and valuable physical insights. Serving as one of the simplest examples of a two-band topological insulator, the one-dimensional SSH model can give rise to exponentially localized edge states under open boundary conditions, which exhibit robustness against disorder and scattering [4–7]. Furthermore, in the thermodynamic limit, two degenerate in-gap topological edge modes can correspond to a nonzero winding number, i.e., the bulk-boundary correspondence relationships [8–11]. Meanwhile, the SSH model and its numerous extensions have been extensively studied to gain insights into a wide range of physical phenomena. Among these extensions, the odd-sized SSH model uniquely exhibits a single, persistent edge state, in contrast to the two edge states observed in even-sized cases. This intriguing phenomenon is commonly referred to as the odd-even effect of the SSH model [8,12,13].

By introducing non-Hermiticity, the interaction between topological insulators and the environment in open systems exhibits more abundant physical phenomenon [14–19] whose theoretical models have been successfully implemented in diverse experimental platforms, including optomechanical systems [11,20–22] and electronic circuits [13,23]. One of the

unique features in non-Hermitian systems is the appearance of complex energy spectra, except for certain systems with parity-time (\mathcal{PT}) symmetry and pseudo-Hermiticity [24–27]. Another intriguing phenomenon in physics is known as the non-Hermitian skin effect (NHSE), where the eigenstates of a system tend to accumulate near the boundaries of a lattice or system. [28–34]. Additionally, the non-Hermitian topological systems incorporating nonreciprocal hopping display intricate band structures and offer valuable physical insights, including non-Hermitian bulk-boundary correspondence relationships and exceptional points [35–43]. However, we should point out that previous works related to the non-Hermitian SSH lattices and their extensions tacitly acknowledged that the edge and skin states should possess an aligned localized direction, yet no one has ever suspected it. Therefore, a crucial question arises: Can the bulk states exhibit an opposite localized direction to that of the edge state in non-Hermitian lattices and under what conditions does this phenomenon occur?

To tackle these inquiries, we investigate the localized directions of edge and skin states in a one-dimensional odd-sized non-Hermitian lattice under open boundary conditions. Our findings demonstrate that the lattice can support four types of edge and skin states, determined by the signs of the directional inverse participation ratio (d_{IPR}), namely, [left-localized edge state (L-E), right-localized skin states (R-S)], [left-localized edge state (L-E), left-localized skin states (L-S)], [right-localized edge state (R-E), left-localized skin states (L-S)], and [right-localized edge state (R-E), right-localized skin states (R-S)], respectively. Our results reveal that the localized directions of the bulk and edge states are respectively determined by the non-Hermitian skin effects and isolated site induced by the odd size of the lattice, resulting

*zhangyunn@hit.edu.cn

†szhang@ybu.edu.cn

‡hfwang@ybu.edu.cn

in the detachment between edge and bulk states. Notably, this phenomenon has not been elucidated in other literature, including the nonreciprocal non-Hermitian even-sized SSH lattices [16,19,31,32], \mathcal{PT} -symmetric non-Hermitian systems [26,27], and non-Hermitian topological lattices with long-range interactions [17,29,39]. To gain a comprehensive understanding of the opposite localization behaviors among eigenstates, we analyze and calculate the boundary conditions governing the localization directions of edge and skin states, which enables us to classify eigenstates into distinct localization types. Importantly, our analytical results closely match the numerical findings, validating the accuracy and validity of our approaches. Furthermore, we expand this unique behavior to trimer non-Hermitian lattices and identify a pair of eigenstates exhibiting opposite localization compared to the skin states. Our research reveals the inherent detachment between edge and skin states in dimer and even multimer non-Hermitian systems with nonreciprocal hopping.

The paper is organized as follows. In Sec. II, we demonstrate the model and Hamiltonian. In Sec. III, the detachment between edge and skin states is analyzed and discussed. In Sec. IV, the analytical and numerical results are investigated. In Sec. V, we extend the detachment between edge and skin states into the trimer and multimer non-Hermitian lattice. Finally, we give the conclusion in Sec. VI.

II. MODEL AND HAMILTONIAN

We consider an odd-sized non-Hermitian SSH model under open boundary conditions, described by the Hamiltonian

$$H = \sum_{j=1}^N [t_L c_{j,A}^\dagger c_{j,B} + t_R c_{j,B}^\dagger c_{j,A}] + \sum_{j=1}^N [v c_{j+1,A}^\dagger c_{j,B} + v c_{j,B}^\dagger c_{j+1,A}], \quad (1)$$

where $c_{j,A}^\dagger$ and $c_{j,B}^\dagger$ are the annihilation (creation) operators for sublattices A and B in the j th cell, respectively. The intracell hopping strengths in opposite directions are denoted as $t_{R(L)} = \lambda(t \pm \Delta)$ and $v = \lambda J$ is the reciprocal intercell hopping strength with $\lambda = 1$ being set as the unit of energy. Here, Δ and J are positive real constants and the total lattice size is $L = 2N + 1$.

The non-Hermitian skin effect arises from the presence of intracell nonreciprocal hopping terms, which leads to the localization of eigenstates at one edge of the lattice. To assess the extension and localization of these eigenstates, we employ the inverse participation ratio $\text{IPR}_n = \sum_{j=1}^L |\psi_{n,j}|^4 / (\langle \psi_n | \psi_n \rangle)^2$. Here $|\psi_n\rangle$ denotes the right eigenstate with component $\psi_{n,j}$ and satisfies $H|\psi_n\rangle = E_n|\psi_n\rangle$, with H being the model Hamiltonian and E_n the n th eigenenergy. Notably, in the thermodynamic limit (L is large enough), the $\text{IPR} \rightarrow 0$ for extended states and $\text{IPR} \rightarrow 1$ for localized states, respectively. However, relying solely on the IPR is insufficient to directly discern the localized directions of the edge and bulk states. Consequently, we introduce the d_{IPR} [37,38] as

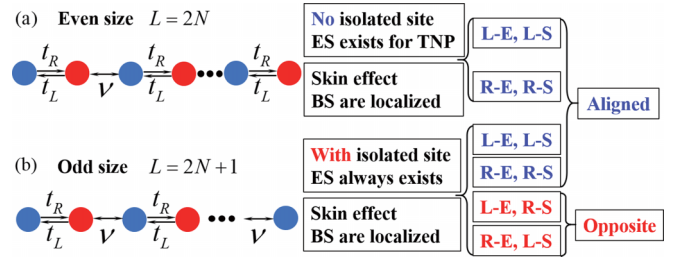


FIG. 1. Schematic diagram of even-sized ($L = 2N$) and odd-sized ($L = 2N + 1$) SSH lattices shown in (a) and (b). The intracell nonreciprocal and intercell reciprocal hoppings are represented as $t_{R(L)} = \lambda(t \pm \Delta)$ and λJ , respectively. The blue and red circles denote sublattices A and B . Here, TNP means topological nontrivial phase. ES and BS correspond the edge and bulk states of system. L-S (E) and R-S (E) denote the left-localized and right-localized skin(edge) states, respectively.

a complementary measure, defined as

$$d_{\text{IPR}}(\psi_n) = \mathcal{P}(\psi_n) \sum_{j=1}^L \frac{|\psi_{n,j}|^4}{(\langle \psi_n | \psi_n \rangle)^2}, \quad (2)$$

where the $\mathcal{P}(\psi_n) = \text{sgn}[\sum_{j=1}^L (j - \frac{L}{2} - \delta) |\psi_{n,j}|]$. Here, the $\text{sgn}(x)$ is positive for $x > 0$ and negative for $x < 0$. The parameter δ satisfies $0 < \delta < 0.5$. $\mathcal{P}(\psi_n)$ encodes the directional information of eigenstates ψ_n , enabling d_{IPR} to discern whether a specific wave function is left-localized or right-localized. In our paper, the positive and negative values of d_{IPR} represent right-localized and left-localized eigenstates, respectively. As an illustration, we demonstrate the eigenenergy spectra characterized by the d_{IPR} in the even-sized non-Hermitian SSH model whose model is shown in Fig. 1(a). The d_{IPR} values for the edge and bulk states consistently exhibit positive values for $t < 0$ and negative values for $t > 0$, respectively, as shown in Figs. 2(a) and 2(b). These findings suggest that the edge and skin states consistently demonstrate an aligned localized direction whose behaviors can also be confirmed from their probability distribution of eigenstates, as shown in Figs. 2(c) and 2(d). Notably, the inherent chiral symmetry of the Hamiltonian leads to a notable phenomenon: altering the signs of both t and Δ produces an equivalent impact on the localized directions of the both edge state and the skin state whose intriguing phenomenon has been meticulously investigated in Ref. [44]. The behavior of eigenstates, characterized by the aligned localized direction of the edge and skin states, can be observed across various even-sized non-Hermitian SSH models and their extensions. However, whether the edge states consistently maintain the aligned localized direction as the skin states in dimer non-Hermitian systems is still unclear.

III. DETACHMENT BETWEEN EDGE AND SKIN STATES

Here, we investigate the behavior of edge and bulk states in an odd-sized non-Hermitian SSH model, as shown in Fig. 1(b). We demonstrate the real and imaginary energy spectrum of the odd-sized non-Hermitian SSH model characterized by the d_{IPR} in Figs. 3(a) and 3(b) in which an

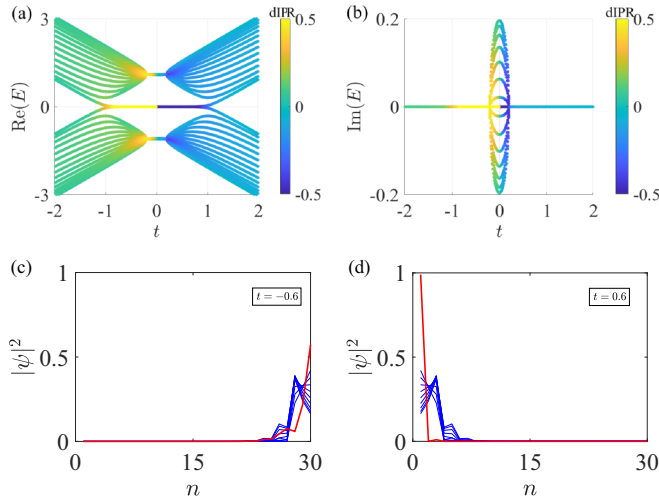


FIG. 2. (a) and (b) show the real and imaginary parts of the energy spectra featured by d_{IPR} under open boundary conditions with the lattice size $L = 30$, in which the color bar of blue ($d_{\text{IPR}} < 0$) and yellow ($d_{\text{IPR}} > 0$) regions denote the left-localized and right-localized eigenstates. (c) and (d) correspond to the distributions of some representative eigenstates with $t = -0.6$ and $t = 0.6$, respectively. The rest parameters are determined as $J = 1.1$, $\Delta = 0.2$, and $\delta = 0.2$.

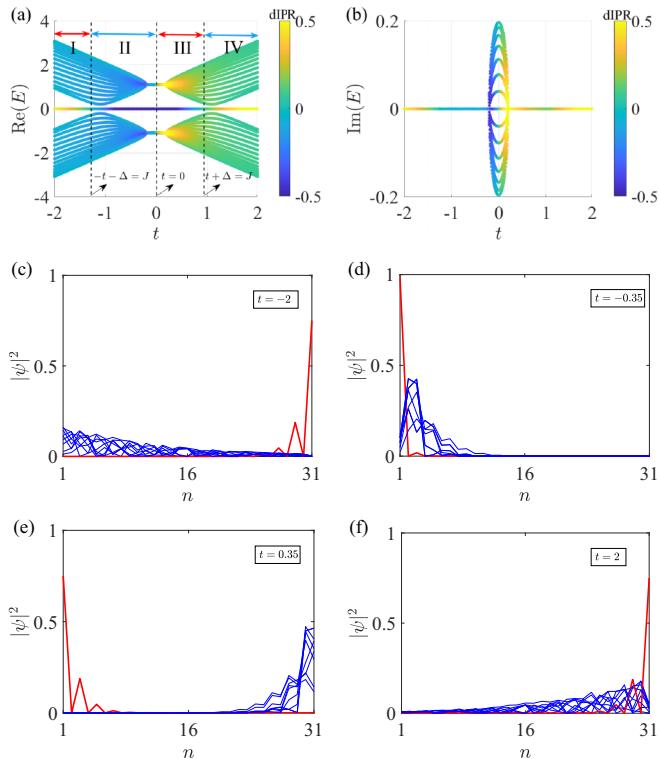


FIG. 3. (a) and (b) demonstrate the real and imaginary parts of the energy spectra featured by d_{IPR} under open boundary conditions with lattice size $L = 31$, in which the color bar of blue ($d_{\text{IPR}} < 0$) and yellow ($d_{\text{IPR}} > 0$) regions denote the left-localized and right-localized eigenstates. [(c)–(f)] correspond to the distributions of some representative eigenstates with $t = -2$, $t = -0.35$, $t = 0.35$, and $t = 2$, respectively. The rest parameters are determined as $J = 1.1$, $\Delta = 0.2$, and $\delta = 0.2$.

ever-present edge state occurs in the band gap as mentioned before. The counterintuitive yet intriguing behaviors are manifested through the signs of d_{IPR} , where the d_{IPR} displays distinct signs for the edge and skin (bulk) states in certain parameter regions, indicating the presence of opposite localizations between the edge and skin states. Subsequently, we further categorize the eigenstates into four distinct regimes of interest based on the signs of d_{IPR} for the edge and skin states.

In regime I, the d_{IPR} values for the edge and skin states maintain opposite signs. Specifically, the edge state exhibits a positive d_{IPR} , while the skin states hold negative d_{IPR} . This phenomenon indicates the detachment between the edge and skin states for $t < -1.3$ ($-t > J + \Delta$). The presence of an isolated site induced by the odd size ensures a right-localized edge state (R-E), while the NHSE drives the bulk states to the left boundary, resulting in left-localized skin states (L-S), namely, R-E and L-S. Moreover, the probability distribution of the edge (red line) and skin states (blue lines) in Fig. 3(c) confirms their right-localized and left-localized behaviors, consistent with the d_{IPR} values in regime I.

In regime II, both the edge and bulk states have negative d_{IPR} values, which indicates that the edge and skin states share the aligned localized direction for $-1.3 < t < 0$ ($0 < -t < J + \Delta$). In this case, the edge state is left-localized (L-E) and the skin states are also left-localized (L-S), namely, L-E and L-S. The presence of the isolated site and the skin effect contributes to the left localization of the edge and bulk states. Furthermore, the probability distributions in Fig. 3(d) show that all eigenstates are left-localized, coinciding with the behaviors of d_{IPR} observed in regime II.

In regime III, resembling regime I, the edge and bulk states exhibit opposite signs of d_{IPR} . However, in this case, the d_{IPR} value for the edge state is negative, while the bulk states exhibit positive d_{IPR} values. This indicates the detachment between the left-localized edge state (L-E) and the right-localized skin states (R-S) for $0 < t < 0.9$ ($0 < t < J - \Delta$), namely, L-E and R-S whose essence is similar to regime I, but with opposite direction. The behaviors of the edge (red line) and skin states (blue lines) in Fig. 3(e) confirm their left-localized and right-localized characteristics, respectively, consistent with the signs of d_{IPR} in regime III.

In regime IV, similar to regime II, both the edge and bulk states maintain positive d_{IPR} values. This implies that the edge state and the bulk states are simultaneously right-localized for $t > 0.9$ ($t > J - \Delta$), namely, R-E and R-S. The presence of the isolated site and the skin effect contributes to the right localization of both the edge and bulk states. In addition, the probability distributions in Fig. 3(f) confirm the right-localized behavior of all eigenstates, consistent with the results in regime IV. Notably, regimes I and III exhibit a counterintuitive phenomenon where the edge state is detached from the skin states, a behavior rarely discussed in other non-Hermitian literature.

IV. NUMERICAL AND ANALYTICAL RESULTS

A. Numerical results

Notably, in the previous chapter, we identified the detachment phenomenon between the edge and bulk states,

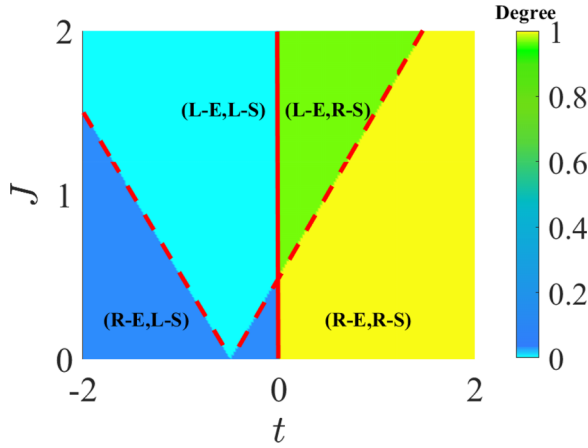


FIG. 4. Phase diagram of the eigenstates' localized direction presents degree of detachment as a function of the parameters t and J with the system size $L = 31$ and $\Delta = 0.2$. There are four different phases. Blue regions denote the opposite localized phase with Degree = $1/L = 0.032$, where only one right-localized eigenstate exists and the rest eigenstates are all left-localized. Cyan region presents the same localized phase with Degree = $0/L = 0$, where all eigenstates are left-localized. Green region denotes the opposite localized phase with Degree = $30/L = 0.968$, where only one eigenstate is left-localized and the rest of the eigenstates are localized on the right boundary. Yellow region presents the same localized phase with Degree = $31/L = 1$, where all eigenstates are right-localized. The red dashed and solid lines are the analytical phase boundaries of the localized directions for the edge and skin states whose results are demonstrated in Eqs. (3) to (5).

but it was limited to a specific parameter regime. It is crucial to note that this finding does not reflect the general behavior observed across all parameter regimes. To further investigate the detachment phenomenon between edge and skin states, the degree of detachment is introduced and defined as Degree = $X_n[d_{\text{IPR}}(\psi_n) > 0] / \{X_n[d_{\text{IPR}}(\psi_n) > 0] + Y_n[d_{\text{IPR}}(\psi_n) < 0]\}$ [37,38], where X_n and Y_n are the number of eigenstates with right-localized and left-localized directions, respectively. A degree of detachment being 1 indicates that all eigenstates are right-localized, while the degree approaching 0 suggests that all eigenstates are left-localized, and no detachment phenomenon occurs. Intermediate degree values between 0 and 1 indicate the presence of the detachment phenomenon between edge and bulk states. Then we show the degree of detachment as a function of t and J in Fig. 4. The parameter plane is divided into four regions: the cyan and yellow regions correspond to Degree = 0 and Degree = 1, respectively, indicating all eigenstates are left or right localization. In addition, the blue and green regions represent the existence of only one right-localized edge state (R-E) and one left-localized edge state (L-E), respectively, indicating the opposite localization between edge and skin states. The detailed values of the degree are demonstrated in the annotation.

B. Analytical results

From an analytical perspective, we can explore the localized behaviors of the edge and skin states and explain the nature of the detachment phenomenon. Two crucial factors

come into play: the edge state determined by the competition between intracell and intercell hopping and the skin states determined by the strength of nonreciprocal hopping [18,28,31,38].

1. Localized direction for edge state

As is widely known, the presence of an isolated site can give rise to the appearance of edge states when the strength of intercell hopping surpasses that of intracell hopping, regardless of the Hermitian or non-Hermitian SSH model. However, for odd-sized lattices, there is always an isolated site irrespective of the hopping strengths. The different hopping regimes between the intracell and intercell result in distinct isolated lattice sites, corresponding to different localized directions for the edge states. When the strength of intercell hopping exceeds the maximum value of the intracell nonreciprocal hopping, a left-localized edge state occurs at the end of the lattice. Conversely, a right-localized edge state appears. These regimes can be described as boundary conditions between the left and right-localized edge states as $J = |\max(t_L, t_R)|$, where a left-localized edge state appears for $J > |\max(t_L, t_R)|$ and a right-localized edge state appears for the opposite case. Specifically, for $J < t + \Delta$ when $t > -\Delta$ and $J < -(t + \Delta)$ when $t < -\Delta$, there is a right-localized edge state. In addition, a left-localized edge state appears while $J > t + \Delta$ and $J > -(t + \Delta)$. These conditions of the localized directions for edge state can be represented as

$$t > -\Delta \begin{cases} -\Delta < t < J - \Delta, & \text{L-E,} \\ t > J - \Delta, & \text{R-E,} \end{cases} \quad (3)$$

$$t < -\Delta \begin{cases} -(J + \Delta) < t < -\Delta, & \text{L-E,} \\ t < -(J + \Delta), & \text{R-E.} \end{cases} \quad (4)$$

The analytical boundary conditions for the existence of left-localized or right-localized edge states are consistent with the numerical results, as the red dashed lines shown in Fig. 4 whose results identify the analytical solutions for the localized direction of the edge state.

2. Localized direction for skin states

For the non-Hermitian skin effect, the behavior of bulk states is closely related with the strength of nonreciprocal hopping, which means that the $\max(|t_L|, |t_R|)$ determines the localized direction of skin states. Left-localized skin states appear when $|t_L| > |t_R|$, while right-localized skin states occur when $|t_R| > |t_L|$. Therefore, the conditions of the localized direction for the skin states can be expressed as

$$\begin{cases} t < 0, & |t - \Delta| > |t + \Delta|, & \text{L-S,} \\ t > 0, & |t + \Delta| > |t - \Delta|, & \text{R-S.} \end{cases} \quad (5)$$

Similarly, the analytical results for the skin states also coincide with the numerical results, as in the red solid line shown in Fig. 4. Furthermore, by combining the analytical solutions for the edge and skin states, we provide their localized conditions under different parameters in Table I. We confirm that the parameter regions for aligned and opposite localized directions correspond precisely to the cyan (yellow) and blue (green) regions, respectively, as labeled in Fig. 4. Moreover, our analytical results demonstrate excellent agreement with the numerical findings.

TABLE I. The localized directions of bulk and skin states are reflected by different nonreciprocal hopping parameters whose results originate from Eqs. (3) to (5). Left and right localizations denote the localized directions of wave functions. Corporate localized directions represent the behavior of all eigenstates in which the opposite and aligned directions indicate the edge and skin states maintain an opposite and aligned localized direction. Parameter regions correspond to the numerical results in Fig. 4 in which the blue (green) and cyan (yellow) regions indicate the existence and disappearance of the detachment phenomenon.

Hopping parameters	Bulk states	Edge states	Corporate localized directions	Parameter regions
$t < -(J + \Delta)$	left localization	right localization	opposite direction	blue region
$-(J + \Delta) < t < -\Delta$	left localization	left localization	aligned direction	cyan region
$t > J - \Delta, t > -\Delta$	left localization	left localization	aligned direction	cyan region
$J - \Delta < t < 0$	left localization	right localization	opposite direction	blue region
$0 < t < J - \Delta$	right localization	right localization	aligned direction	yellow region
$t > J - \Delta, t > 0$	right localization	left localization	opposite direction	green region

V. DETACHMENT PHENOMENA IN MULTIMER NON-HERMITIAN LATTICE

The non-Hermitian SSH model and its various extensions have been widely explored to reveal novel physical phenomena whose each unit cell contains two sublattices [26,31,33,34]. For comparison, we call it the SSH3 or SSHN models when each cell contains three or more sublattices [45,46]. Here, we extend our exploration to a trimer non-Hermitian SSH3 model under open boundary conditions whose model schematic illustration is demonstrated in Fig. 5. The non-Hermitian Hamiltonian with intracell nonreciprocal hopping can be written as ($\lambda = 1$ is omitted)

$$\begin{aligned}
 H_{\text{tri}} = & \sum_{j=1}^N [(t_1 + \gamma)A_j^\dagger B_j + (t_1 - \gamma)B_j^\dagger A_j] \\
 & + \sum_{j=1}^N [t_2 B_j^\dagger C_j + t_2 C_j^\dagger B_j] \\
 & + \sum_{j=1}^{N-1} [T C_j^\dagger A_{j+1} + T A_{j+1}^\dagger C_j], \quad (6)
 \end{aligned}$$

where $A_j^{(\dagger)}$, $B_j^{(\dagger)}$, and $C_j^{(\dagger)}$ are the annihilation (creation) operators for sublattices A , B , and C in the j th cell, respectively. The reciprocal intercell hopping is represented by T , and the intracell reciprocal and nonreciprocal hopping strengths are denoted as t_2 and $t_1 \pm \gamma$, respectively. Here, γ , t_2 , and T are positive real constants. Similar to the previous analysis, we examine the behavior of eigenstates by analyzing the real and imaginary parts of energy spectra characterized by d_{IPR} . The results divide the behaviors of eigenstates into four regions, as shown in Figs. 6(a) and 6(b), where the regions indicated by blue arrows exhibit an aligned localized direction among eigenstates, while the regions indicated by red arrows display the opposite localized directions. For the regions denoted by

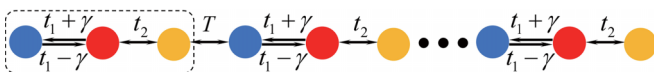


FIG. 5. Schematic diagram of trimer SSH lattice. The intracell hoppings denote as $(t_1 \pm \gamma)$ and t_2 ; the intercell hoppings are represented as T . All of the hoppings are in units of $\lambda = 1$. The blue, red, and yellow circles denote sublattices A , B , and C , respectively.

blue arrows, i.e., $t_1 < -0.5$ and $0 < t_1 < 0.94$, the d_{IPR} s of the eigenstates maintain aligned signs and all eigenstates are left-(right-)localized. This is evident from the probability distributions shown in Figs. 6(c) and 6(e) for their left-localized and right-localized behaviors, respectively. In contrast, for the regions denoted by red arrows, i.e., $-0.5 < t_1 < 0$ and $t_1 > 0.94$, a pair of eigenstates exhibit opposite signs of d_{IPR} compared to the other eigenstates and the edge states support the opposite localized directions with the skin states. This behavior can also be reflected from the probability distributions

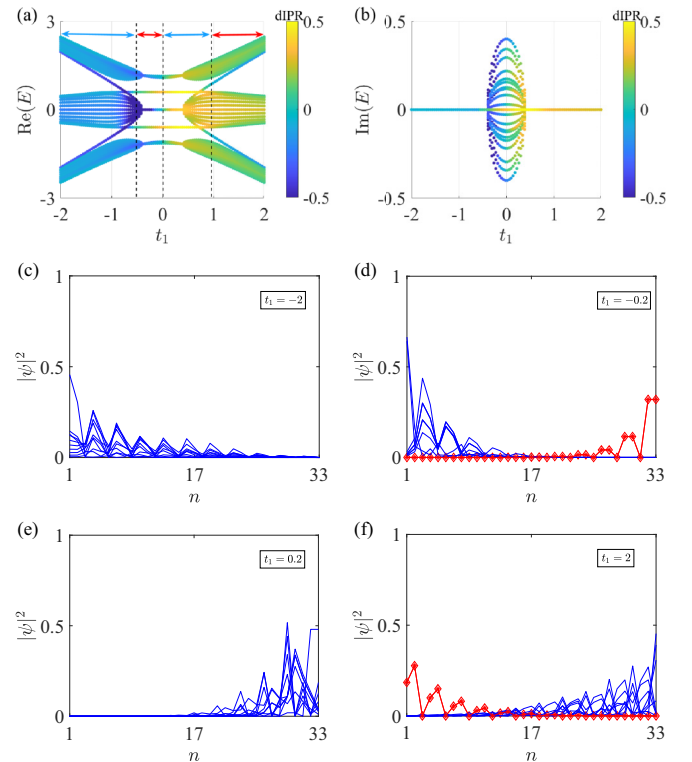


FIG. 6. (a) and (b) show the real and imaginary parts of the energy spectra featured by d_{IPR} for H_{tri} under open boundary conditions with lattice size $L = 33$, in which the color bar of blue [$d_{\text{IPR}}(\psi_n) < 0$] and yellow [$d_{\text{IPR}}(\psi_n) > 0$] regions denote the left-localized and right-localized eigenstates. [(c)–(f)] correspond to the distributions of some representative eigenstates with $t_1 = -2$, $t_1 = -0.2$, $t_1 = 0.2$, and $t_1 = 2$, respectively. The rest parameters are determined as $t_2 = 0.6$, $T = 1$, $\gamma = 0.4$, and $\delta = 0.2$.

in Figs. 6(d) and 6(f), where left-localized skin states and a pair of right-localized edge states are observed in Fig. 6(d), while right-localized skin states and a pair of left-localized bound states are observed in Fig. 6(f). These results indicate the existence of the detachment phenomenon among the eigenstates in the trimer non-Hermitian system.

It is important to note two aspects: First, unlike the detachment between the edge and skin states in the dimer non-Hermitian system, a pair of opposite localized eigenstates appear with respect to the trimer case, and the detachment phenomenon can also occur for the bulk states. Second, the opposite and aligned localization among eigenstates can also be observed in the imaginary parts of the energy spectrum featured by d_{IPR} . These findings demonstrate the presence of detachment between eigenstates in multimetric non-Hermitian lattices. Our work reveals the detachment phenomenon among eigenstates and enriches our understanding of the localized directions of eigenstates in non-Hermitian physics.

VI. CONCLUSION

In conclusion, we investigate the nonreciprocal non-Hermitian odd-sized SSH lattice and reveal the nature of detachment between the edge and skin states. We begin with the spectrum featured by d_{IPR} and analyzed the eigenstates of the even-sized non-Hermitian SSH lattice, laying the foundation for exploring the detachment between the edge and skin states. By analyzing the spectrum and eigenstates of

the odd-sized system, we identify four types of eigenstates based on the signs of d_{IPR} for the edge and skin states: [L-E, R-S], [L-E, L-S], [R-E, L-S], and [R-E, R-S]. Our results reveal that the localized directions of bulk and edge states are subject to skin effects and isolated site induced by odd size, respectively. The signs of d_{IPR} further confirmed the existence of detachment between the edge and skin states. Moreover, the analytical solutions provide compelling evidence for the presence of aligned and opposite localized orientations between the edge and skin states whose findings are in excellent agreement with the numerical results, further supported by the degree of detachment. In the trimer non-Hermitian lattice, we also observe the detachment phenomenon, where a pair of eigenstates exhibit opposite localized directions compared to the skin states. This intriguing discovery emphasizes the occurrence of detachment phenomenon among eigenstates in the trimer non-Hermitian lattice. Overall, our study reveals the intriguing detachment phenomenon between the edge and bulk states in the dimer odd-sized non-Hermitian SSH lattice. This significant finding provides compelling evidence for the existence of detachment in multimetric non-Hermitian lattices.

ACKNOWLEDGMENT

This work was supported by the National Natural Science Foundation of China under Grants No. 12074330, No. 12375020, No. 62071412, No. 62201493, and No. 62301472.

-
- [1] L. Fu, C. L. Kane, and E. J. Mele, Topological insulators in three dimensions, *Phys. Rev. Lett.* **98**, 106803 (2007).
 - [2] M. Z. Hasan and C. L. Kane, Colloquium: Topological insulators, *Rev. Mod. Phys.* **82**, 3045 (2010).
 - [3] X. L. Qi and S. C. Zhang, Topological insulators and superconductors, *Rev. Mod. Phys.* **83**, 1057 (2011).
 - [4] W. P. Su, J. R. Schrieffer, and A. J. Heeger, Solitons in polyacetylene, *Phys. Rev. Lett.* **42**, 1698 (1979).
 - [5] B. A. Bernevig, T. L. Hughes, and S. C. Zhang, Quantum spin Hall effect and topological phase transition in HgTe quantum wells, *Science* **314**, 1757 (2006).
 - [6] H. Takayama, Y. R. Lin-Liu, and K. Maki, Continuum model for solitons in polyacetylene, *Phys. Rev. B* **21**, 2388 (1980).
 - [7] S. Ryu, A. P. Schnyder, A. Furusaki, and A. W. W. Ludwig, Topological insulators and superconductors: Tenfold way and dimensional hierarchy, *New J. Phys.* **12**, 065010 (2010).
 - [8] L. H. Li, Z. H. Xu, and S. Chen, Topological phases of generalized Su-Schrieffer-Heeger models, *Phys. Rev. B* **89**, 085111 (2014).
 - [9] L. Wang, M. Troyer, and X. Dai, Topological charge pumping in a one-dimensional optical lattice, *Phys. Rev. Lett.* **111**, 026802 (2013).
 - [10] M. A. Metlitski, C. L. Kane, and M. P. A. Fisher, Bosonic topological insulator in three dimensions and the statistical Witten effect, *Phys. Rev. B* **88**, 035131 (2013).
 - [11] L. J. Lang, X. Cai, and S. Chen, Edge states and topological phases in one-dimensional optical superlattices, *Phys. Rev. Lett.* **108**, 220401 (2012).
 - [12] C. Wang, L. H. Li, J. B. Gong, and Y. X. Liu, Arbitrary entangled state transfer via a topological qubit chain, *Phys. Rev. A* **106**, 052411 (2022).
 - [13] F. Mei, G. Chen, L. Tian, S. L. Zhu, and S. T. Jia, Robust quantum state transfer via topological edge states in superconducting qubit chains, *Phys. Rev. A* **98**, 012331 (2018).
 - [14] H. Shen, B. Zhen, and L. Fu, Topological band theory for non-Hermitian Hamiltonians, *Phys. Rev. Lett.* **120**, 146402 (2018).
 - [15] S. Yao, F. Song, and Z. Wang, Non-Hermitian chern bands, *Phys. Rev. Lett.* **121**, 136802 (2018).
 - [16] Z. P. Gong, Y. Ashida, K. Kawabata, K. Takasan, S. Higashikawa, and M. Ueda, Topological phases of non-Hermitian systems, *Phys. Rev. X* **8**, 031079 (2018).
 - [17] X. X. Bao, G. F. Guo, and L. Tan, Exploration of the topological properties in a non-Hermitian long-range system, *J. Phys.: Condens. Matter* **33**, 465403 (2021).
 - [18] N. Okuma, K. Kawabata, K. Shiozaki, and M. Sato, Topological origin of non-Hermitian skin effects, *Phys. Rev. Lett.* **124**, 086801 (2020).
 - [19] L. Jin and Z. Song, Bulk-boundary correspondence in a non-Hermitian system in one dimension with chiral inversion symmetry, *Phys. Rev. B* **99**, 081103(R) (2019).
 - [20] M. Ezawa, Nonlinear non-Hermitian higher-order topological laser, *Phys. Rev. Res.* **4**, 013195 (2022).
 - [21] H. Zhao, P. Miao, M. H. Teimourpour, S. Malzard, R. El-Ganainy, H. Schomerus, and L. Feng, Topological hybrid silicon microlasers, *Nat. Commun.* **9**, 981 (2018).

- [22] Y. Lumer, Y. Plotnik, M. C. Rechtsman, and M. Segev, Self-localized states in photonic topological insulators, *Phys. Rev. Lett.* **111**, 243905 (2013).
- [23] J. Cao, X. X. Yi, and H. F. Wang, Band structure and the exceptional ring in a two-dimensional superconducting circuit lattice, *Phys. Rev. A* **102**, 032619 (2020).
- [24] J. Li, A. K. Harter, J. Liu, L. de Melo, Y. N. Joglekar, and L. Luo, Observation of parity-time symmetry breaking transitions in a dissipative Floquet system of ultracold atoms, *Nat. Commun.* **10**, 855 (2019).
- [25] S. Xia, D. Kaltsas, D. Song, I. Komis, J. Xu, A. Szameit, H. Buljan, K. G. Makris, and Z. Chen, Nonlinear tuning of \mathcal{PT} symmetry and non-Hermitian topological states, *Science*. **372**, 72 (2021).
- [26] B. G. Zhu, R. Lü, and S. Chen, \mathcal{PT} symmetry in the non-Hermitian Su-Schrieffer-Heeger model with complex boundary potentials, *Phys. Rev. A* **89**, 062102 (2014).
- [27] Z. H. Xu, R. Zhang, S. Chen, L. B. Fu, and Y. B. Zhang, Fate of zero modes in a finite Su-Schrieffer-Heeger model with \mathcal{PT} symmetry, *Phys. Rev. A* **101**, 013635 (2020).
- [28] H. Jiang, L. J. Lang, C. Yang, S. L. Zhu, and S. Chen, Interplay of non-Hermitian skin effects and Anderson localization in nonreciprocal quasiperiodic lattices, *Phys. Rev. B* **100**, 054301 (2019).
- [29] Z. X. Zhang, R. Huang, L. Qi, Y. Xing, Z. J. Zhang, and H. F. Wang, Topological phase transition and eigenstates localization in a generalized non-hermitian su-schrieffer-heeger model, *Ann. Phys. (Leipzig)* **533**, 2000272 (2021).
- [30] S. Longhi, Self-healing of non-hermitian topological skin modes, *Phys. Rev. Lett.* **128**, 157601 (2022).
- [31] S. Yao and Z. Wang, Edge states and topological invariants of non-hermitian systems, *Phys. Rev. Lett.* **121**, 086803 (2018).
- [32] C. H. Lee and R. Thomale, Anatomy of skin modes and topology in non-Hermitian systems, *Phys. Rev. B* **99**, 201103(R) (2019).
- [33] L. J. Lang, Y. J. Wend, Y. H. Zhang, E. H. Cheng, and Q. X. Liang, Dynamical robustness of topological end states in non-reciprocal Su-Schrieffer-Heeger models with open boundary conditions, *Phys. Rev. B* **103**, 014302 (2021).
- [34] P. M. Gunnink, B. Flebus, H. M. Hurst, and R. A. Duine, Nonlinear dynamics of the non-Hermitian Su-Schrieffer-Heeger model, *Phys. Rev. B* **105**, 104433 (2022).
- [35] L. J. Lang, S. L. Zhu, and Y. D. Chong, Non-Hermitian topological end breathers, *Phys. Rev. B* **104**, L020303 (2021).
- [36] K. Mochizuki, K. Mizuta, and N. Kawakami, Fate of topological edge states in disordered periodically driven nonlinear systems, *Phys. Rev. Res.* **3**, 043112 (2021).
- [37] Q. B. Zeng and R. Lü, Real spectra and phase transition of skin effect in nonreciprocal systems, *Phys. Rev. B* **105**, 245407 (2022).
- [38] Q. B. Zeng, Non-Hermitian skin effect edge, *Phys. Rev. B* **106**, 235411 (2022).
- [39] F. K. Kunst, E. Edvardsson, J. C. Budich, and E. J. Bergholtz, Biorthogonal bulk-boundary correspondence in non-hermitian systems, *Phys. Rev. Lett.* **121**, 026808 (2018).
- [40] V. M. Martinez Alvarez, J. E. Barrios Vargas, and L. E. F. Foa Torres, Non-Hermitian robust edge states in one dimension: Anomalous localization and eigenspace condensation at exceptional points, *Phys. Rev. B* **97**, 121401(R) (2018).
- [41] C. Yin, H. Jiang, L. Li, R. Lü, and S. Chen, Geometrical meaning of winding number and its characterization of topological phases in one-dimensional chiral non-Hermitian systems, *Phys. Rev. A* **97**, 052115 (2018).
- [42] M. J. Ablowitz, C. W. Curtis, and Y. P. Ma, Linear and nonlinear traveling edge waves in optical honeycomb lattices, *Phys. Rev. A* **90**, 023813 (2014).
- [43] D. Leykam and Y. D. Chong, Edge solitons in nonlinear-photonic topological insulators, *Phys. Rev. Lett.* **117**, 143901 (2016).
- [44] J. Yogesh N, Mapping between Hamiltonians with attractive and repulsive potentials on a lattice, *Phys. Rev. A* **82**, 044101 (2010).
- [45] D. Xie, W. Gou, T. Xiao, B. Gadway, and B. Yan, Topological characterizations of an extended Su-Schrieffer-Heeger model, *npj Quantum Inf.* **5**, 55 (2019).
- [46] Y. He and C. C. Chien, Non-Hermitian generalizations of extended Su-Schrieffer-Heeger models, *J. Phys.: Condens. Matter* **33**, 085501 (2021).